# THEME ARTICLE: COMPUTATIONAL MODELING OF ICE SHEETS AND GLACIERS

## A Finite-Element-Based Cohesive Zone Model of Water-Filled Surface Crevasse Propagation in Floating Ice Tongues

Yuxiang Gao <sup>10</sup>, Vanderbilt University, Nashville, TN, 37235, USA
Gourab Ghosh <sup>10</sup>, Hexagon Manufacturing Intelligence, Novi, MI, 48377, USA
Stephen Jiménez, Corvid Technologies, Mooresville, NC, 28117, USA
Ravindra Duddu <sup>10</sup>, Vanderbilt University, Nashville, TN, 37235, USA

We present a finite-element-based cohesive zone model for simulating the nonlinear fracture process driving the propagation of water-filled surface crevasses in floating ice tongues. The fracture process is captured using an interface element whose constitutive behavior is described by a bilinear cohesive law, and the bulk rheology of ice is described by a nonlinear elasto-viscoplastic model. The additional loading due to meltwater pressure within the crevasse is incorporated by combining the ideas of poromechanics and damage mechanics. We performed several numerical studies to explore the parametric sensitivity of surface crevasse depth to ice rheology, cohesive strength, density, and temperature for different levels of meltwater depth. We find that viscous (creep) strain accumulation promotes crevasse propagation and that surface crevasses propagate deeper in ice shelves/tongues if we consider depth-varying ice density and temperature profiles. Therefore, ice flow models must account for depth-varying density and temperature-dependent viscosity to appropriately describe calving outcomes.

ce tongues and ice shelves are the floating extensions of ice sheets, which provide buttressing to the upstream land ice and control the ice mass loss into the ocean. Iceberg calving resulting from the propagation of crevasses and rifts is a predominant mass loss mechanism in ice shelves and ice tongues. Incidentally, meltwater can infiltrate surface crevasses (or seawater can infiltrate basal crevasses) and apply additional hydraulic pressure on the crevasse walls promoting crevasse propagation deeper into the glacier; this hydraulic-pressure-driven fracture is generally referred to as hydrofracture. To better understand crevasse propagation in relation to different physical and environmental conditions that can lead to diverse calving styles, it is crucial that we develop and utilize advanced fracture-process-based models.

1521-9615 © 2023 IEEE
Digital Object Identifier 10.1109/MCSE.2023.3315661
Date of publication 4 October 2023; date of current version 25 October 2023.

In the glaciology literature, three broad classes of models are used for estimating crevasse penetration depths: zero stress, linear elastic fracture mechanics (LEFM), and continuum damage mechanics (CDM). The zero-stress model provides the simplest treatment of fracture by assuming that ice has zero tensile strength and that a crevasse will penetrate to the depth at which the longitudinal stress becomes zero. Existing analytical calving laws based on zero stress and LEFM models suffer from a few limitations: 1) the tensile strength of ice, which inherently determines the length scale of the fracture process zone at the crevasse tip is disregarded, based on the concept of small-scale yielding; 2) the analytical stress and stress intensity factor are calculated assuming idealized rectangular bodies and simplistic boundary conditions, which are not representative of the geometry or boundary conditions of real ice shelves/ tongues;<sup>2</sup> and 3) the assumption of brittle fracture ignores the contribution of time-dependent creep

deformation in promoting fracture and altering calving outcomes.

To overcome the aforementioned limitations, CDM models were developed and utilized for predicting crevasse depth.<sup>3</sup> The presence of a substantial distributed region of damage near the crack tip, known as the *fracture process zone*, introduces nonlinearity in fracture scaling, necessitating the use of a quasi-brittle (nonlinear and nonlocal) representation of the fracture. Incorporating nonlocal CDM models into the shallow shelf approximation can enable physically consistent simulation of the calving process from ice shelves,<sup>4</sup> compared to analytical calving laws based on ice thickness, height-above-buoyancy, or stress/strain-rate invariants.<sup>5,6</sup>

Nonlocal CDM models<sup>3</sup> can account for the propagation of water-filled crevasses assuming a quasistatic hydrofracture process by including the effect of meltwater pressure in crevasses as an additional crack-opening stress. However, phenomenological CDM models involve empirical parameters, and existing experiments and observations may not be adequate to uniquely calibrate these parameters, which can contribute to uncertainty. Alternatively, phase-field damage models can be used for simulating glacier calving,<sup>7</sup> wherein the model parameters are related to fracture toughness and material strength measured from standard experiments. However, nonlocal CDM and phasefield models are computationally expensive as fine meshes are required to adequately resolve the damage length scale.

Cohesive zone models (CZMs) are a class of CDMs that have been extensively used for simulating fracture in composite materials and hydraulic fracture in poroelastic rock. In a CZM, crack propagation is determined based on cohesive strength and fracture energy (two parameters) per fracture mode, unlike in LEFM models, where crack propagation is determined based on the fracture energy (only one parameter). In our past work,8 we verified and validated the damage-based CZM implementation for composite fracture. Here, we extend this CZM for simulating the propagation of air/water-filled surface crevasses in ice shelves/ tongues, assuming nonlinear elasto-viscoplastic ice rheology. We utilize the poro-damage approximation<sup>3</sup> that combines the ideas of Biot's theory of poroelasticity with damage mechanics, based on the assumption that isotropic damage can be treated as porosity. We use this poro-damage CZM to estimate crevasse penetration depths, compare them with the estimates from the LEFM model, and examine the sensitivity of predicted depths to ice rheology, cohesive strength, density, and temperature.

## **MODEL FORMULATION**

#### Finite-Element-Based CZM

To describe the formulation of the CZM, we consider an idealized 2-D rectangular ice shelf/tongue domain  $\Omega$ subdivided into rectangular finite elements, as shown in Figure 1. The pre-existing crevasse (red line in Figure 1) and the cohesive interface  $\Gamma_*$  (blue line in Figure 1), representing the potential crevasse path, split the bulk domain  $\Omega$  into two nonoverlapping subdomains:  $\Omega^{(1)}$ and  $\Omega^{(2)}$ . We use a rectangular Cartesian coordinate system and the total Lagrangian description with coordinates  $\mathbf{x} = \{x, y, z\}$ , assuming small deformations. The displacement field  $\mathbf{u}(\mathbf{x})$  is discontinuous across the cohesive interface  $\Gamma_*$ , but continuous within the subdomains  $\Omega^{(1)}$  and  $\Omega^{(2)}$ , so it can be represented by two separate continuous functions  $\mathbf{u}^{(1)}$  and  $\mathbf{u}^{(2)}$ , respectively. The interface separation vector is defined by the nodal displacements of the cohesive element as

$$\Delta = [[\mathbf{u}]] = \mathbf{u}^{(2)} - \mathbf{u}^{(1)}.$$
 (1)

The interface traction/stress vector  $\mathbf{t}_{\rm c}$  is defined as a function of the interface separation

$$\mathbf{t}_{\mathrm{c}} = \alpha(\Delta)\Delta$$
 (2)

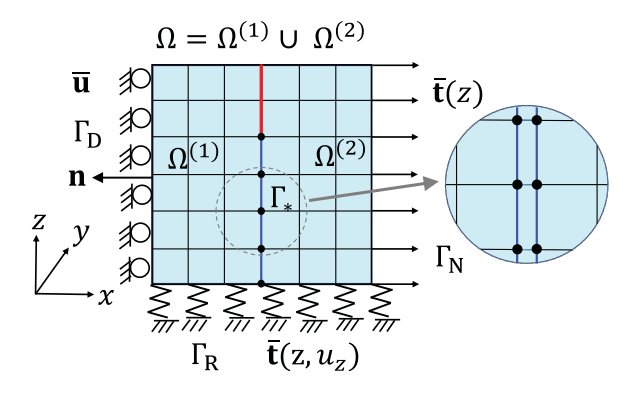


FIGURE 1. Schematic of the ice domain with the cohesive elements placed at the crevasse interface (refer to the "Finite-Element-Based CZM" and "Static Equilibrium" sections for notation and domain definitions). The red line represents the pre-existing crevasse, where the cohesive elements are fully damaged. The blue line represents the potential crevasse interface, where the cohesive elements are either partially damaged or undamaged. The crack is allowed to grow only along the blue line, so we only capture vertical mode I crevasse propagation. The zoomed-in view shows the nodes of the interface element, which are the edge nodes of adjacent bulk finite elements. In the undeformed or initial configuration, the cohesive element has zero thickness.

where  $\alpha$  is the nonlinear cohesive stiffness matrix. The aforementioned traction-separation relationship, otherwise called *cohesive law*, describes the constitutive equation of the cohesive elements governing crack initiation and propagation.

#### Bilinear Mixed-Mode Cohesive Law

The bilinear cohesive law describes an initial (increasing) linear elastic response followed by a (decreasing) linear damage-induced softening response. For mixed-mode fracture under quasi-static loading in 2-D, we can express this cohesive law in the damage mechanics framework, as detailed in our previous work. The tangential  $t_{\tau}$  and normal  $t_{n}$  components of the interface traction vector  $\mathbf{t}_{c}$  are related to the tangential  $\Delta_{\tau}$  (sliding or mode II) and normal  $\Delta_{n}$  (opening or mode I) components of the interface separation vector  $\Delta$  as

where

$$lpha_{ au} = (1 - D_{\mathrm{s}}) lpha_{ au}^{0}; \, lpha_{\mathrm{n}} = \left(1 - D_{\mathrm{s}} \frac{\langle \Delta_{\mathrm{n}} \rangle}{\Delta_{\mathrm{n}}}\right) lpha_{\mathrm{n}}^{0}$$
 (4)

 $\alpha_n^0$  and  $\alpha_\tau^0$  represent the initial cohesive stiffness in the normal and the tangential directions, respectively, and  $D_s$  is the scalar damage variable. In (4), the Macaulay brackets are defined such that  $\langle \Delta_n \rangle = \max(0, \Delta_n),$  which ensures that there is no damage growth or damage effect on the normal traction under compression or contact.

The scalar damage variable  $D_{\rm s}$  is defined by

$$D_{\mathrm{s}} = \begin{cases} 0 & \text{if} \quad \Delta_{\mathrm{e}} < \Delta_{\mathrm{e}}^{\mathrm{c}}, \\ \frac{\Delta_{\mathrm{e}}^{\mathrm{u}} (\Delta_{\mathrm{e}} - \Delta_{\mathrm{e}}^{\mathrm{c}})}{\Delta_{\mathrm{e}} (\Delta_{\mathrm{e}}^{\mathrm{u}} - \Delta_{\mathrm{e}}^{\mathrm{c}})} & \text{if} \quad \Delta_{\mathrm{e}}^{\mathrm{c}} \leq \Delta_{\mathrm{e}} < \Delta_{\mathrm{e}}^{\mathrm{u}} \\ 1 & \text{if} \quad \Delta_{\mathrm{e}}^{\mathrm{u}} \leq \Delta_{\mathrm{e}} \end{cases}$$
 (5)

where the equivalent separation  $\Delta_e=\sqrt{\left<\Delta_n\right>^2+\Delta_\tau^2}.$  In (5), the critical and ultimate interface separation parameters  $\Delta_e^c$  and  $\Delta_e^u$  are defined based on strength and fracture energy considerations as

$$\begin{split} &\frac{1}{\Delta_{\rm e}^{\rm c}} = \sqrt{\left(\frac{\alpha_{\rm n}^{\rm 0} \mathbf{cos}I}{\sigma_{\rm max}}\right)^2 + \left(\frac{\alpha_{\rm \tau}^{\rm 0} \mathbf{cos}II}{\tau_{\rm max}}\right)^2},\\ &\frac{1}{\Delta_{\rm e}^{\rm u}} = \left(\frac{\alpha_{\rm n}^{\rm 0} \Delta_{\rm e}^{\rm c} (\mathbf{cos}I)^2}{2~G_{IC}}\right) + \left(\frac{\alpha_{\rm \tau}^{\rm 0} \Delta_{\rm e}^{\rm c} (\mathbf{cos}II)^2}{2~G_{IIC}}\right) \end{split} \tag{6}$$

where the direction cosines  $\cos I = \Delta_{\rm n}/\Delta_{\rm e}$  and  $\cos II = \Delta_{\tau}/\Delta_{\rm e},~\sigma_{\rm max}$  and  $\tau_{\rm max}$  are the pure mode I (tensile) and mode II (shear) cohesive strengths, respectively; and  $G_{IC}$  and  $G_{IIC}$  are the pure mode I and mode II critical fracture energies, respectively. A sketch of the bilinear

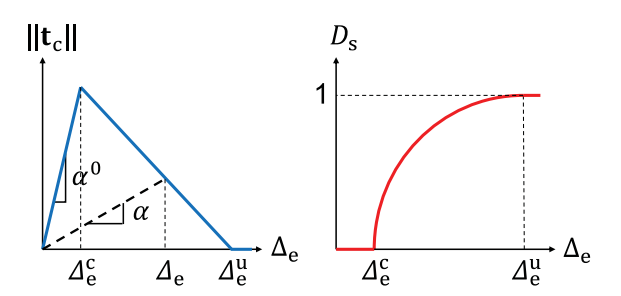


**FIGURE 2.** Sketch of the bilinear CZM for mixed-mode fracture. (a) A traction-separation relationship and (b) damage-separation relationship. For a given mode-mix ratio, the equivalent or resultant traction is given by the magnitude of the traction vector  $||\mathbf{t}_{\rm c}|| = \sqrt{t_{\rm n}^2 + t_{\rm \tau}^2}$ , and the equivalent separation is defined as  $\Delta_{\rm e} = \sqrt{\langle \Delta_{\rm n} \rangle^2 + \Delta_{\rm \tau}^2}$ . Note that the interface damage  $D_{\rm s}$  is zero until the separation reaches a critical value and then increases rapidly (nonlinearly) until failure.

traction-separation and damage-separation relationships is shown in Figure 2.

## Poro-Damage Extension for Hydrofracture

We extend the aforementioned bilinear cohesive law to model the fracture of air-filled surface crevasses to account for the hydrofracture of water-filled surface crevasses. The scalar (isotropic) damage variable can be interpreted as the ratio of the area of voids to the total area of the 2-D planar cohesive interface. As meltwater fills the crevasse, we assume that water can seep into the damaged zone below the crevasse tip and exert hydrostatic pressure to pry open the crevasse. To account for this additional pressure load, we previously developed the continuum poro-damage mechanics approach,3 which extends the ideas of Biot's theory of poroelasticity by assuming isotropic damage to have a similar effect on the material behavior as porosity. Noting that interface traction is equal to the stress vector corresponding to the crack surface, the poro-damage mechanics approach can be applied to the CZM. The water pressure  $p_{\rm w}$  within the crevasse and its damage process zone can be introduced into the bilinear cohesive law in (3) to obtain the extended cohesive law for hydrofracture as

The depth-varying water pressure is defined by

$$p_{\rm w}(z) = \rho_{\rm w} g \langle h_{\rm s} - (z - z_{\rm s}) \rangle \tag{8}$$

where  $\rho_{\rm w}$  is the density of meltwater, g is the acceleration due to gravity,  $z_{\rm s}$  is the height of the surface

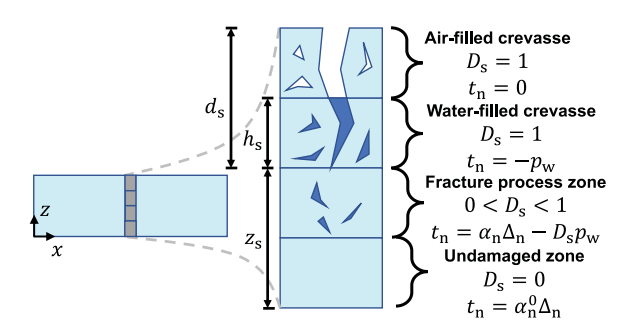


FIGURE 3. Schematic diagram of the predominantly mode I fracture of an air/water-filled crevasse in the ice domain, as described by the poro-damage CZM. The interface elements inserted into the finite-element mesh account for the damage growth process through the scalar damage variable  $D_{\rm s}$ . The crevasse depth measured from the top of the ice slab is  $d_{\rm s}$ , and  $h_{\rm s}$  is the height of the meltwater column measured from the crevasse tip. For any given  $d_{\rm s}$  and  $h_{\rm s}$ , four different interface zones can be identified, including an air-filled and water-filled crevasse, fracture process zone, and undamaged zone based on the damage variable.

crevasse tip from the base of the ice slab, and  $h_s$  is the height of the meltwater column measured from the crevasse tip.

Figure 3 depicts the process of crevasse propagation described by the CZM. The potential crevasse path described by the cohesive region consists of interface elements that connect the neighboring bulk finite elements. As the ice slab deforms and creeps under the action of gravity, in some cohesive elements, the normal traction at the crack tip will reach the cohesive strength, as the interface separation reaches a critical value under predominantly mode I fracture. Subsequently, damage (in the form of microcracks or microvoids) grows within these cohesive interface elements, and meltwater will percolate into the damaged regions assuming a fully saturated medium. In this scenario, four different types of cohesive interface states can be perceived:

- 1) Air-filled crevasse: The interface element is fully damaged  $(D_{\rm s}=1)$  and there is no meltwater pressure  $(p_{\rm w}=0),$  so the normal interface traction becomes zero  $(t_{\rm n}=0).$
- 2) Water-filled crevasse: The interface element is fully damaged and meltwater applies pressure on the crack walls  $(p_{\rm w}>0)$ , so the normal interface traction magnitude is equal to that of the water pressure at that depth  $(t_{\rm n}=-p_{\rm w})$ .
- 3) Fracture process zone: The interface element is partially damaged  $(0 < D_{\rm s} < 1)$  with distributed

- microcracks/microvoids that are saturated with meltwater, so the normal interface traction includes contributions from the interface cohesion and water pressure  $(t_{\rm n}=\alpha_{\rm n}\Delta_{\rm n}-D_{\rm s}p_{\rm w})$ .
- 4) Undamaged zone: The interface element has no damage  $(D_{\rm s}=0)$ , so the normal interface traction is linearly proportional to the interface separation with the undamaged cohesive stiffness  $(t_{\rm n}=\alpha_{\rm n}^0\Delta_n)$ .

Thus, the poro-damage mechanics enables the automated handling of air/water-filled crevasse propagation using cohesive elements.

BY SWITCHING ON AND OFF THE VISCOUS STRAIN CONTRIBUTIONS IN THIS MODEL, WE CAN EXAMINE THE DIFFERENCES IN FRACTURE PROPAGATION AND CALVING OUTCOMES FOR PURELY ELASTIC AND ELASTO-VISCOPLASTIC RHEOLOGIES.

#### Constitutive Model for Glacier Ice

The mechanical response of glacier ice is dependent on the strain rate (nonlinear), temperature, and time. Over longer time scales, glacier and ice-sheet flow is described using a nonlinear viscous Stokes model based on Glen's law; whereas, over shorter time scales, the mechanical response is often described by linear elastic or linear/nonlinear visco-elasto-plastic constitutive models. Additionally, due to the Arrhenius-type temperature dependence of ice's viscosity, temperature gradients in ice can introduce significant changes in flow rates and stress state. Here, we utilize the temperature-dependent elasto-viscoplastic constitutive model for polycrystalline ice.9 By switching on and off the viscous strain contributions in this model, we can examine the differences in fracture propagation and calving outcomes for purely elastic and elastoviscoplastic rheologies.

We assume small deformations as crevasse propagation generally occurs over shorter time scales. Consequently, the total strain tensor can be additively decomposed as

$$\epsilon = \epsilon^{\mathrm{e}} + \epsilon^{\mathrm{v}}$$
 (9)

where  $\epsilon^e$  and  $\epsilon^v$  denote the elastic and viscous strain tensors, respectively. The total strain tensor is given by

the symmetric part of the displacement gradient tensor as

$$\epsilon = \frac{1}{2}(\nabla \mathbf{u} + \nabla \mathbf{u}^T) \tag{10}$$

where  $\nabla$  denotes the gradient operator and T in the superscript denotes a transpose. The elastic stress-strain relationship in the bulk finite elements is given by the generalized Hooke's law as

$$\sigma = \mathbf{C} : \epsilon^{\mathbf{e}}$$
 (11)

where : denotes the double dot or inner product, C denotes the fourth-order isotropic elasticity tensor, whose components are defined in terms of Young's modulus E and Poisson's ratio  $\nu$ . The viscous strain rate is given by the power-law creep equation as

$$\dot{\epsilon}^{\mathrm{v}} = \frac{\partial \epsilon^{\mathrm{v}}}{\partial t} = \frac{3}{2} K_N(T) \sigma_{\mathrm{e}}^{(N-1)/2} \sigma^{\mathrm{dev}}$$
 (12)

where  $K_N(T)$  is the temperature-dependent viscosity coefficient; N is the viscous exponent; the equivalent stress measurement  $\sigma_{\rm e}=3/2\,\sigma^{\rm dev}$ ;  $\sigma^{\rm dev}$ ; and  $\sigma^{\rm dev}$  denotes the deviatoric part of the Cauchy stress tensor.

WE PERFORM A SERIES OF NUMERICAL SIMULATIONS USING THE PORO-DAMAGE CZM TO EXAMINE THE PROPAGATION OF AIR/WATER-FILLED SURFACE CREVASSES IN IDEALIZED ICE TONGUES/SHELVES.

### Static Equilibrium

The stress state in the glacier is obtained by solving the governing equations of static equilibrium along with the boundary conditions

$$\nabla \cdot \boldsymbol{\sigma} + \mathbf{b} = \mathbf{0} \quad \text{in} \quad \Omega \tag{13}$$

$$\mathbf{u} = \bar{\mathbf{u}} \ \ \mathrm{on} \ \ \Gamma_{\mathrm{D}}$$
 (14)

$$\bar{\mathbf{t}}(z) = \rho_{\mathrm{sw}} g \langle h_{\mathrm{w}} - z \rangle$$
 on  $\Gamma_{\mathrm{N}}$  (15)

$$\bar{\mathbf{t}}(z,u_z) = \rho_{\rm sw} g \langle h_{\rm w} - z - u_z \rangle$$
 on  $\Gamma_{\rm R}$  (16)

where  $\mathbf{b} = [0,0,-\rho_{\mathrm{i}}g]^T$  is the body force,  $\rho_{\mathrm{i}}$  is ice density,  $\rho_{\mathrm{sw}}$  is seawater density,  $\bar{\mathbf{u}}$  is the prescribed displacement on the Dirichlet boundary  $\Gamma_{\mathrm{D}}$ ,  $\bar{\mathbf{t}} = \sigma \mathbf{n}$  is the prescribed traction on the Neumann boundary  $\Gamma_{\mathrm{N}}$ , and  $\mathbf{n}$  is the outward unit normal to the boundary  $\Gamma \equiv \partial \Omega$ . On the Robin boundary  $\Gamma_{\mathrm{R}}$ , the traction is equal to the buoyancy pressure, which depends on seawater height  $h_{\mathrm{w}}$  and vertical displacement  $u_z$ .

## **Numerical Implementation**

We implement the poro-damage-based CZM in the commercial software ABAQUS via the User ELement (UEL) and User MATerial (UMAT) subroutines. The Fortran codes and input files are available for download at https://doi.org/10.15784/601704. At the cohesive interface, we deploy four-noded zero-thickness interface elements with a two-point Gaussian integration scheme to capture crevasse propagation. By design, the mesh size (or node spacing) is equal to the interface element size near the cohesive interface and is gradually coarsened away from it toward the domain boundaries to reduce the computation expense. We choose interface element sizes small enough so that there are at least three elements within the estimated cohesive process zone;8 this ensures an accurate representation of the stress distribution within the fracture process zone at the crevasse tip. The UEL subroutine describes the computation of the force vector and stiffness matrix for the interface element. In the bulk regions, we deploy four-noded plane strain continuum elements (i.e., bilinear quadrilateral) with a four-point Gaussian integration scheme to capture elasto-viscoplastic ice deformation. The initial stress state in the glacier is established using a linear elastic step, and subsequent isochoric viscoplastic deformations are determined by assuming appropriate time steps using explicit time updates. The UMAT subroutine describes the computation of the stiffness matrix and the righthand side force vector for the bulk finite elements.

## SIMULATION RESULTS

#### Geometry and Boundary Conditions

We perform a series of numerical simulations using the poro-damage CZM to examine the propagation of air/water-filled surface crevasses in idealized ice tongues/shelves. We consider a simple rectangular geometry with an L=5 km (length) and H=125 m (height) under plane strain assumptions, as depicted in Figure 4. A free-slip (roller) boundary condition is applied to the left edge to prevent horizontal motion. A Robin-type boundary condition is applied to the bottom edge to simulate a buoyant ice shelf/tongue. Seawater pressure is applied as a Neumann boundary condition at the right edge (terminus) with seawater level  $h_{\rm w}=\rho_{\rm i}/\rho_{\rm sw}H$ , which is the floating depth.

#### Ice Properties and Model Parameters

The material parameters of the incompressible, linear elastic rheology case are the Young's modulus E=9500 MPa and Poisson's ratio  $\nu=0.4995$ . The parameters of the nonlinear viscoplastic rheology case are the viscosity

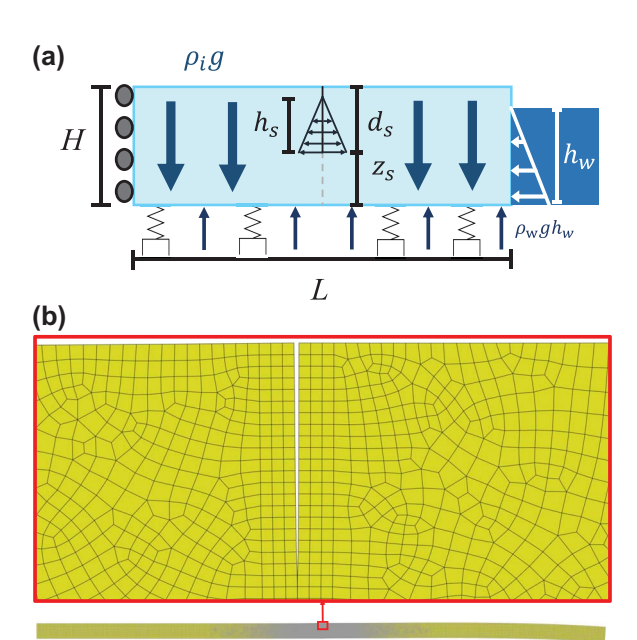


**FIGURE 4.** (a) Loading configuration for the idealized ice shelf with height H=125 m and length L=5 km. (b) Finite-element mesh used for analysis. The size of the zoomed-in domain is roughly 11 m  $\times$  20 m.

coefficient  $K_N = 1.58825 \times 10^{-7}$  Pa-s at  $T = -10^{\circ}\mathrm{C}$  and viscosity exponent parameter N=3. The density of ice, meltwater, and seawater are  $\rho_{\rm i} = 917$  kg/m³,  $\rho_{\rm w} =$  $1000 \text{ kg/m}^3$ , and  $\rho_{sw} = 1020 \text{ kg/m}^3$ . Based on previous studies, 10 we assumed fracture toughness  $K_{IC} = 0.4$ MPa $\sqrt{m}$  and mode I cohesive strength  $\sigma_{max}$  in the range of 35-220 kPa. We then determined  $G_{IC}=$  $K_{IC}^2 (1-\nu^2)/E = 12.63$  N/m. Due to the lack of experimental data on mode II properties, we assumed  $G_{IC} = G_{IIC}$  and  $\sigma_{\max} = \tau_{\max}$ . Because we only study predominantly mode I crevasse propagation in idealized rectangular floating ice tongues, the crevasse depth predictions are not sensitive to the choice of  $G_{IIC}$  and  $\tau_{\rm max}$ . The initial cohesive stiffnesses  $\alpha_{\rm n}^0 =$  $\alpha_{\tau}^0 = 10^{10} \text{ N/m}^3$  are treated as penalty parameters, so we assumed them to be large enough to enforce displacement continuity across the crack interface before fracture without affecting numerical convergence.

## Effect of Ice Rheology and Cohesive Strength on Crevasse Propagation

It has been argued that the nonlinear viscous nature of glacier ice and its finite (tensile/shear) cohesive strength are important parameters to be incorporated into calving laws. Therefore, we first investigate the effect of ice rheology and strength on the penetration depth of

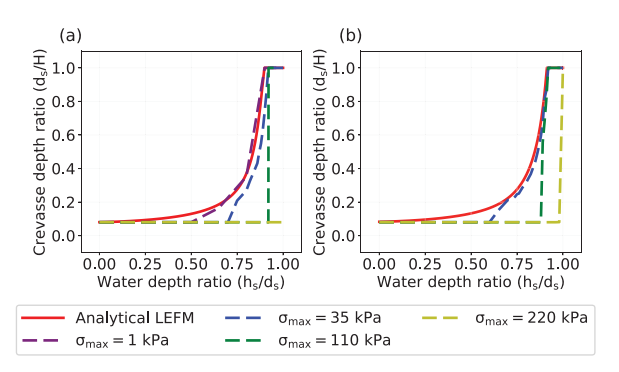
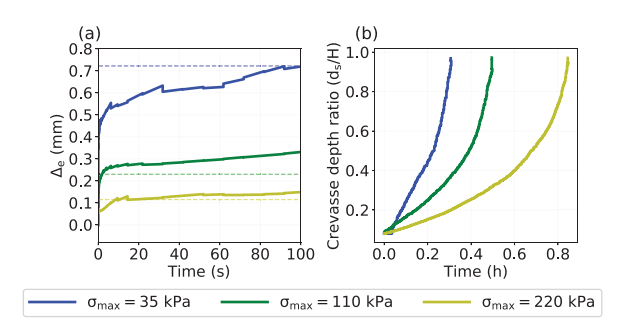


FIGURE 5. Surface crevasse penetration depth ratios  $(d_{\rm s}/H)$  in the idealized ice shelf for different meltwater depth ratios  $(h_{\rm s}/d_{\rm s})$  predicted using the CZM for different cohesive strengths (dashed lines). Crevasse depth ratios are evaluated assuming (a) linear elastic rheology and (b) nonlinear elastoviscoplastic rheology and compared with those from an analytical LEFM model (solid line). Note that as cohesive strength goes to zero  $(\sigma_{\rm max}=1~{\rm kPa})$ , the CZM predicted crevasse depths for the linear elastic rheology converges to the LEFM model predictions.

air/water-filled surface crevasses in the idealized ice tongue. We assume three values of cohesive strength: 35 kPa, 110 kPa, and 220 kPa, which are within the range of values reported in the literature. 10,11 We consider linear elastic and nonlinear elasto-viscoplastic rheology for glacier ice and compare the CZM-predicted crevasse depths for different strengths with the analytical LEFM solution, 10 as shown in Figure 5.

In the case of linear elastic rheology [Figure 5(a)], we find that for the small cohesive strengths of 1 kPa and 35 kPa, the predicted crevasse depths from the CZM matches best with the LEFM result. If the crevasse is partially filled with meltwater, then the CZM does not predict crevasse propagation for meltwater depth ratio  $h_s/d_s < 0.65$ ; whereas for  $h_s/d_s > 0.65$ , the crevasse depth gradually increases with meltwater depth until it fully penetrates the ice thickness at  $h_{\rm s}/d_{\rm s}\approx 0.9$ . For the medium strength of 110 kPa, the CZM result does not show a gradual increase in crevasse depth; rather, it predicts that the crevasse will not propagate if  $h_{\rm s}/d_{\rm s} < 0.9$  but fully penetrates the ice shelf if  $h_s/d_s > 0.9$ . For the nonlinear elastoviscoplastic rheology [Figure 5(b)], the CZM mostly predicts similar crevasse propagation behavior as the linear elastic rheology. However, the time-dependent creep deformation promotes crevasse propagation for slightly smaller meltwater depth ratios. Notably, for the large strength of 220 kPa, the CZM result with the nonlinear elasto-viscoplastic rheology shows that a



**FIGURE 6.** Time evolution of (a) equivalent separation in the crevasse tip element and (b) crevasse depth ratio  $(h_{\rm s}/d_{\rm s}=1)$  for the idealized ice shelf obtained from the CZM for different cohesive strengths. The critical separation threshold for corresponding cohesive strength is shown by the dashed lines in (a). The nonlinear elasto-viscoplastic rheology accounts for creep deformation, which gradually opens the subcritical crevasse and promotes deeper crevasse penetration, eventually leading to calving (i.e.,  $d_{\rm s}/H=1$ ).

fully water-filled crevasse penetrates the entire ice tongue/shelf thickness; whereas with the linear elastic rheology, the surface crevasses will not propagate even if it is fully filled with meltwater.

We further explore the role of viscous creep deformation in promoting crevasse propagation to answer a key fracture mechanics question: Why do crevasses propagate to a greater depth for smaller meltwater depth ratios with the nonlinear elasto-viscoplastic rheology? Noting that crevasse propagation described by damage evolution  $D_{\rm s}$  in the cohesive element is dependent on the equivalent separation  $\Delta_e$  [see (5) and (6)], we plotted the equivalent separation and crevasse depth ratio versus time in an element near the crevasse tip in Figure 6(a) and (b), respectively. It is apparent that the equivalent separation is initially less than the critical separation required for damage evolution as the normal traction at the crevasse tip is smaller than the cohesive strength. However, time-dependent creep deformation will gradually increase the interface separation over the critical limit and lead to damage evolution and crevasse propagation. In contrast, if the linear elastic rheology is assumed, the equivalent separation will not increase with time, so crevasse propagation in the ice shelf would be arrested for the larger cohesive strength. The time scale associated with water-filled crevasse propagation in a floating ice tongue [minutes to an hour in Figure 6(b)] is much smaller compared to its flow or deformation (days to years), given that typical strain rates are  $10^{-7}-10^{-9}$  per second. Therefore, the assumption of small strain is reasonable to assess the effect of small amounts of accumulated viscous strain on crevasse propagation.

## Effect of Depth-Varying Density and Temperature Profiles on Crevasse Propagation

The upper regions of glaciers and ice tongues typically consist of firn, which is partially compacted granular snow and an intermediate state between snow and glacial ice. The near-surface density of firn is considerably smaller ( $\approx$ 350 kg/m<sup>3</sup>) than that of solid ice ( $\approx$ 917 kg/m<sup>3</sup>).<sup>10</sup> In the case of an ice shelf, both density and temperature vary with depth, and the latter is due to the fact the bottom surface is in contact with seawater. whereas the top surface is in contact with air. For simplicity, we assume that the temperature varies linearly with depth, where the bottom temperature is  $-5^{\circ}$ C and the top surface temperature is  $-30^{\circ}$  C. The temperature dependence of glacier ice viscosity is incorporated into the constitutive model using the Arrhenius law.9 We considered the empirical relationship from the literature 10 to describe the variation of ice density with depth. We performed a set of simulations using the CZM with three different cohesive strengths (i.e., 35 kPa, 110 kPa, and 220 kPa) for air-filled (dry) and 90% water-filled crevasse cases. In all the following simulations, we use the nonlinear elasto-viscoplastic model for ice and take the initial seed crevasse to be 10 m long (i.e., the initial crevasse depth ratio is 0.08). For the constant temperature and density simulations, we took  $T = -10^{\circ}$ C and  $\rho_i = 917$  kg/m<sup>3</sup>.

The final crevasse depth ratios are reported in Tables 1 and 2. We find that in both the air-filled crevasse and 90% water-filled crevasse cases, the crevasse depth ratio for a given cohesive strength is the largest if the depth variation of both temperature and density is considered. Table 1 shows that with constant density, the driving force is not large enough to

TABLE 1. Effect of density and temperature on final air-filled crevasse depth ratio in ice tongues.

σ <sub>max</sub> (kPa)	Constant $ au$ Constant $ ho_{ m i}$	Constant $T$ Variable $ ho_{ m i}$	Variable $T$ Constant $ ho_{\mathrm{i}}$	Variable $ au$ Variable $ ho_{ m i}$
35	0.08	0.1328	0.08	0.2912
110	0.08	0.1872	0.08	0.3072
220	0.08	0.1888	0.08	0.3088

TABLE 2. Effect of density and temperature on final 90% water-filled crevasse depth ratio in ice tongues.

σ <sub>max</sub> (kPa)	Constant $ au$ Constant $ ho_{ extsf{i}}$	Constant $T$ Variable $ ho_{\rm i}$	Variable $T$ Constant $ ho_{\mathrm{i}}$	Variable $ au$ Variable $ ho_{ m i}$
35	0.816	1	0.8631	1
110	0.68	1	0.7208	1
220	0.08	1	0.7528	1

propagate the crevasse beyond the initial crevasse with or without variable temperature. However, for variable density cases, the driving force is large enough to propagate the crevasse for both constant and variable temperature cases. Moreover, we get the deepest crevasses for the variable density and temperature case because the temperature dependence of viscosity further alters the stress state to promote crevasse propagation. From Table 2, we find that the 90% water-filled crevasse can fully penetrate the ice shelf if depth variation of density  $\rho_i$  is considered, thus leading to a different calving outcome. Thus, the assumption of constant density and temperature overestimates crevasse closure, so crevasse depth is underestimated.  $^{10}$ 

With variable density, in the air-filled crevasse case, crevasse depth slightly increases as the cohesive strength is increased (Table 1); whereas in the 90% water-filled crevasse cases, the crevasse fully penetrates the ice shelf irrespective of the value of the cohesive strength (Table 2). In both cases, the effect of cohesive strength on crevasse propagation is less significant for calving outcomes compared to other variables, namely, meltwater depth, density, and temperature. However, more parametric studies are needed to study the influence of depth-varying Young's modulus and fracture toughness on the penetration depth of water-filled surface crevasses.<sup>12</sup> In the supplementary material, which is available in the IEEE Computer Society Digital Library at http://doi.ieeecomputersociety.org/10.1109/MCSE.2023.3315561, we also compared crevasse propagation in ice shelves with the same mass (Tables S1 and S2), as opposed to ice shelves with the same height reported here.

### CONCLUSION

We developed a new poro-damage mechanics-based CZM for simulating nonlinear and time-dependent crevasse propagation in glaciers driven by thermohydromechanical processes. In this CZM formulation, the scalar damage variable represents the ratio of the isotropic void area to the total area on the cohesive crack interface. Assuming meltwater can permeate

the damaged material and exert hydrostatic pressure along the interface, we defined the effective normal traction in the cohesive element based on Biot's theory of poroelasticity. A limitation of our simple finite-element-based CZM implementation (in the commercial software ABAQUS) is its reliance on predefined potential crack paths; however, it is adequate for studying predominantly mode I propagation of water-filled crevasses, which is comparable to LEFM and zero stress-based crevasse models.

Through several simulation studies, we examined the influence of ice rheology, cohesive strength, depthvariable density, and temperature profiles on crevasse penetration depth in ice tongues/shelves. Our key finding is that temperature-dependent viscous (creep) deformation and depth-varying ice density promote crevasse propagation and can alter calving outcomes. Our studies suggest that ice flow models and calving laws must appropriately incorporate/parameterize the effects of variable ice density, in addition to that of temperature-dependent viscosity. To conclude, our CZM model will be useful for determining ice cohesive strength at fracture initiation as appropriate experimental/ field data become available and provides a nonlinear alternative to LEFM that is more computationally efficient than phase-field fracture models. In our future studies, we will also examine depth variation of Young's modulus and fracture toughness on crevasse propagation<sup>12</sup> and attempt to develop a new calving parameterization for shallow ice shelves, which can be deployed in large-scale ice sheet models.

## **ACKNOWLEDGMENT**

This work was supported by the National Science Foundation's Office of Polar Programs under CAREER Grant PLR-1847173 and NASA Cryosphere Award 80NSSC21K1003.

#### REFERENCES

 M. E. Mobasher, R. Duddu, J. N. Bassis, and H. Waisman, "Modeling hydraulic fracture of glaciers using continuum damage mechanics," J. Glaciol., vol. 62, no. 234, pp. 794–804, 2016, doi: 10.1017/jog.2016.68.

- S. Jimenez and R. Duddu, "On the evaluation of the stress intensity factor in calving models using linear elastic fracture mechanics," J. Glaciol., vol. 64, no. 247, pp. 759–770, 2018, doi: 10.1017/jog.2018.64.
- R. Duddu, S. Jimenez, and J. Bassis, "A non-local continuum poro-damage mechanics model for hydrofracturing of surface crevasses in grounded glaciers," J. Glaciol., vol. 66, no. 257, pp. 415–429, Jun. 2020, doi: 10.1017/jog.2020.16.
- A. Huth, R. Duddu, and B. Smith, "A generalized interpolation material point method for shallow ice shelves. Part II: Anisotropic nonlocal damage mechanics and rift propagation," J. Adv. Model. Earth Syst., vol. 13, no. 8, Aug. 2021, Art. no. e2020MS002292, doi: 10.1029/2020MS002292.
- W. H. Lipscomb et al., "Description and evaluation of the community ice sheet model (CISM) v2. 1," Geoscientific Model Develop., vol. 12, no. 1, pp. 387–424, 2019, doi: 10.5194/gmd-12-387-2019.
- M. J. Hoffman et al., "MPAS-Albany Land Ice (MALI): A variable-resolution ice sheet model for Earth system modeling using Voronoi grids," *Geoscientific* Model Develop., vol. 11, no. 9, pp. 3747–3780, 2018, doi: 10.5194/gmd-11-3747-2018.
- X. Sun and R. Duddu, "A poro-damage phase field model for hydrofracturing of glacier crevasses," Extreme Mechanics Lett., vol. 45, May 2021, Art. no. 101277, doi: 10.1016/j.eml.2021.101277.
- G. Ghosh, R. Duddu, and C. Annavarapu, "A stabilized finite element method for enforcing stiff anisotropic cohesive laws using interface elements," *Comput. Methods Appl. Mechanics Eng.*, vol. 348, pp. 1013–1038, May 2019, doi: 10.1016/j.cma.2019.02.007.
- R. Duddu and H. Waisman, "A temperature dependent creep damage model for polycrystalline ice," Mechanics Mater., vol. 46, pp. 23–41, Mar. 2012, doi: 10.1016/j.mechmat.2011.11.007.
- C. J. Van der Veen, "Fracture mechanics approach to penetration of surface crevasses on glaciers," *Cold Regions Sci. Technol.*, vol. 27, no. 1, pp. 31–47, 1998, doi: 10.1016/S0165-232X(97)00022-0.
- E. Ultee, C. Meyer, and B. Minchew, "Tensile strength of glacial ice deduced from observations of the 2015 eastern Skaftá cauldron collapse, Vatnajökull ice cap,

- Iceland," J. Glaciol., vol. 66, no. 260, pp. 1024–1033, 2020, doi: 10.1017/jog.2020.65.
- M. A. Rist, P. R. Sammonds, H. Oerter, and C. S. M. Doake, "Fracture of Antarctic shelf ice," J. Geophys. Res., Solid Earth, vol. 107, no. B1, pp. ECV 2-1–ECV 2-13, Jan. 2002, doi: 10.1029/2000JB000058.

YUXIANG GAO is a graduate student at Vanderbilt University, Nashville, TN, 37235, USA. His research interests include computational solid mechanics, damage mechanics, physics-informed machine learning, and finite element method. Gao received his B.S. degree in engineering mechanics from Harbin Institute of Technology. Contact him at yuxiang.gao@vanderbilt.edu.

GOURAB GHOSH is an applications engineer at Hexagon Manufacturing Intelligence, Novi, MI, 48377, USA. His research interests are in the field of computational solid mechanics with an emphasis on modeling fracture, and additive manufacturing process simulation of composite materials. Ghosh received his Ph.D. degree in civil engineering from Vanderbilt University. Contact him at gourab.ghosh@hexagon.com.

STEPHEN JIMÉNEZ is an engineering analyst and developer at Corvid Technologies, Mooresville, NC, 28117, USA. His research interests are in the field of computational solid mechanics, fluid dynamics, and heat transfer, with an emphasis on coupled multi-physics modeling. Jiménez received his Ph.D. degree in civil engineering from Vanderbilt University. Contact him at stephen.k.jimenez@vanderbilt.edu.

RAVINDRA DUDDU is an associate professor at Vanderbilt University, Nashville, TN, 37235, USA. His research interests are in the area of computational physics and mechanics, with a focus on the development of advanced computational approaches for predicting damage evolution in materials, involving fracture, corrosion and phase change. Duddu received his Ph.D. degree in civil engineering from Northwestern University. Contact him at ravindra.duddu@vanderbilt.edu.